Research in Astronomy and Astrophysics, 25:065021 (10pp), 2025 June https://doi.org/10.1088/1674-4527/add566
CSTR: 32081.14.RAA.add566

Polarization Profiles of Globular Cluster Pulsars from FAST. I. 25 Profiles from Previously Known Pulsars

Tong Liu[1,2], Lin Wang[3,4], and Zhichen Pan[1,2,5,6]
[1] National Astronomical Observatories, Chinese Academy of Sciences, Beijing 100101, China
[2] College of Astronomy and Space Sciences, University of Chinese Academy of Sciences, Beijing 100049, China
[3] Shanghai Astronomical Observatory, Chinese Academy of Sciences, Shanghai 200030, China; wanglin@shao.ac.cn
[4] Kavli Institute for Astronomy and Astrophysics, Peking University, Beijing 100871, China
[5] CAS Key Laboratory of FAST, National Astronomical Observatories, Chinese Academy of Sciences, Beijing 100101, China
[6] Guizhou Radio Astronomical Observatory, Guizhou University, Guiyang 550025, China
Received 2025 January 8; revised 2025 April 29; accepted 2025 May 6; published 2025 June 4

Abstract

We present a polarization study of 25 globular cluster (GC) pulsars observed with the Five-hundred-meter Aperture Spherical radio Telescope (FAST), including 15 profiles measured for the first time. The pulse width–period relationships for millisecond pulsars (MSPs) in GCs follow power-law indices of −0.268 (W10) and −0.330 (W50), consistent with normal pulsars. Only 20% of the sample exhibit clear S-shaped position angle curves-significantly fewer than in the normal pulsar population. Rotation Measures (RMs) for these pulsars suggest that GCs near the Galactic plane show higher RMs, in agreement with former studies. Polarization ratios were measured, with M53A showing the highest linear polarization (56%) and M15H the highest absolute circular polarization (37%). On average, GC pulsars exhibit lower circular (−1%) and absolute circular (11%) polarization compared to normal pulsars observed with Parkes (5% and 32%, respectively). However, their polarization distributions align with MSPs in the Galactic plane, suggesting GC environments do not drastically alter emission properties.

Key words: (stars:) pulsars: general – (Galaxy:) globular clusters: general – polarization

1. Introduction

Pulsars are among the most highly polarized astrophysical sources in the universe (Lyne & Smith 1968). These polarization properties and the shape of their profiles are closely tied to the radiation mechanisms and magnetic field structures of pulsars. For instance, the rotation vector model (RVM; Radhakrishnan & Cooke 1969) offers a theoretical framework for interpreting the variation of polarization position angles (PAs) across pulse phases, particularly in slow pulsars. These pulsars are typically characterized by spin periods exceeding 30 ms and often undergoing a recycling phase. This model is grounded in the geometry of the pulsar's magnetic field and its orientation relative to the emission beam, providing critical insights into the emission mechanisms and magnetic field structure of these objects. Expanding upon this, the core and cone model (Lyne & Manchester 1988) explains the observed polarization and intensity profiles in terms of core and conal emission components within the pulsar's radio beam. Furthermore, the patchy beam model (Karastergiou & Johnston 2007) explores the relationship between the radial emission height and the resulting pulse shape, offering insights into the complex structure of pulsar emission regions.

Rotation Measure (RM), derived from polarization measurements, describes the polarization angle change as radio waves propagate through the interstellar medium. This makes pulsars one of tracers to study the Galactic magnetism along the line of sight (Manchester 1974). The current understanding of Galactic magnetic field structure has been largely shaped by observations of both slow pulsars and millisecond pulsars (MSPs) distributed along the Galactic plane (GP) and halo. Early foundational work by Manchester (1974) pioneered Galactic magnetic field mapping using RMs from 19 pulsars. Subsequent studies, such as those by Ng et al. (2020) utilizing RMs from 80 pulsars, demonstrated that line-of-sight magnetic field strengths align with the estimated average Galactic magnetic field strength. Most recently, the MeerKAT Thousand-Pulsar-Array (TPA) project has significantly advanced this field, providing RM measurements for 1097 pulsars (Oswald et al. 2025). These studies support the hypothesis that the large-scale Galactic magnetic field exhibits a bisymmetric spiral structure that closely traces the Galactic spiral arms. These investigations have mainly targeted pulsars within the GP, while largely excluding globular cluster (GC) pulsars, which are primarily distributed in the halo of our galaxy.

Since the discovery of the first GC pulsar, J1824-2452A, by Lyne et al. (1987), over 340 pulsars have been reported in 45 GCs.[7] A polarization census of GC pulsars offers a powerful probe for investigating the formation and evolution of

[7] https://www3.mpifr-bonn.mpg.de/staff/pfreire/GCpsr.html

magnetic field structures within GCs and magnetic field in the halo surrounding the Galaxy (e.g., Ferrière & Terral 2014). Polarimetric studies of pulsars in 47 Tucanae (NGC 104) have yielded particularly compelling results. Abbate et al. (2020) demonstrated a characteristic bending of the Galactic magnetic field induced by the intracluster medium. Abbate et al. (2022) subsequently identified clear signatures of small-scale magnetic turbulence within the cluster. Beyond 47 Tucanae (NGC 104), comprehensive polarimetric surveys have been extended to additional globular clusters in the southern celestial hemisphere. Notable examples include detailed polarization studies of pulsars in Terzan 5, which reveals that the Galactic magnetic field varies at sub-parsec scales (Martsen et al. 2022). In contrast to GCs in the southern sky, systematic polarimetric studies of northern GC pulsars remain scarce, primarily due to their intrinsically faint emission characteristics and the limited sensitivity of observations. This observational gap underscores the critical need for high-sensitivity polarimetric campaigns, which are now uniquely enabled by large telescopes like FAST and SKA, to precisely characterize the polarization properties of these elusive pulsar populations.

Furthermore, pulsars residing in GCs often experience unique evolutionary processes due to the highly dynamic and dense environments within GCs, including frequent stellar collisions and gravitational interactions (Rappaport et al. 1989). This raises an interesting question: do pulsars in GCs exhibit polarization properties similar to those outside GCs? Current understanding remains insufficient to conclusively address this question, highlighting the need for further investigation into the polarization characteristics of GC pulsars.

The advent of the Five-hundred-meter Aperture Spherical radio Telescope (FAST; Nan et al. 2011) has significantly improved the sensitivity of pulsar observations, enabling more precise measurements for pulsar polarization. A study of single-pulse polarization of PSR B1929+10 helps the analysis of a periodic modulation of the pulsar (Kou et al. 2021), further demonstrating FAST's exceptional sensitivity. More studies have been conducted with FAST, such as polarization measurements of the Chinese pulsar timing array (Xu et al. 2025) and a survey of polarization of 682 pulsars (Wang et al. 2023). Meanwhile, FAST also improves the studies of GC pulsars. Among the 93 pulsars discovered in 17 GCs within the FAST sky, more than two-thirds were discovered by FAST.[8] Timing solutions have been made for more than 70 pulsars such as the recently reported in NGC 6517 (Yin et al. 2024) and M3 (Li et al. 2024). However, only 11 polarization profiles of these 93 pulsars have been measured to date (e.g.,Pan et al. 2023 and Wang et al. 2023).

[8] e.g., see, https://fast.bao.ac.cn/cms/article/65/.

Here, we present polarization profile measurements of 25 pulsars in GCs, including 15 measured for the first time as our first results from continuing timing and monitoring GC pulsars with FAST. All these 25 pulsars were discovered before FAST. Our work provides samples for studying pulsar magnetic field structures, emission mechanisms, and the magnetic field properties of GCs. Observations and data acquisition are described in Section 2, with data reduction in Section 3. Results and discussion are presented in Section 4, followed by conclusions given in Section 5.

2. Observations and Data Acquisition

In the FAST sky, 27 GC pulsars were discovered before FAST construction completion. These pulsars have undergone long-term timing measurements, and 90% of these exhibit signal-to-noise ratios (S/N) greater than 10 with our data sets, allowing us to obtain their polarization profiles and precise measurements.

As our first phase of work, we processed the data of 25 pulsars from eight GCs including M53 (M53A), M3 (M3A, B, and D), M5 (M5A to E), NGC 6517 (NGC 6517A to D), NGC 6539 (NGC 6739A), NGC 6760 (NGC 6760A and B), M71 (M71A) and M15 (M15A to H). Two candidate sources, M3C and NGC 6749B, were excluded from our sample as they were only detected in single epochs and could not be confirmed as genuine pulsars through follow-up observations (e.g., Li et al. 2024).

The data used in this work were observed using the 19-beam receiver of FAST, covering a frequency range of 1–1.5 GHz. The signals were channelized and digitized using a Reconfigurable Open Architecture Computing Hardware (ROACH)[9] unit. Then, the data were subsequently packetized and stored in search mode PSRFITS format including four polarizations (AA, BB, AB, BA). The channel bandwidth and sampling time of the data were 122 kHz and 49.152 μs, respectively. The detailed information of FAST receiver system, such as system temperature, sky coverage, etc., can be found in Jiang et al. (2020). At the beginning of each observation, a 1-minute noise diode signal was injected with period of 0.2 s. The integration of each observation was decided by the decl. of the GCs in the sky. We observed each GC as longer time as we can to achieve higher S/N. The source and observation details can be found in Table 1.

3. Data Reduction

3.1. Polarization Calibration

The signals from both noise diode and pulsars were folded into sub-integrations using the software package DSPSR (van Straten & Bailes 2011). The length of the sub-integration is 60 s.

[9] Developed by the Collaboration for Astronomy Signal Processing and Electronics Research (CASPER) group; http://casper.berkeley.edu/.

Table 1
FAST GC Observations and Data References for Polarization Measurements

GC	Date	R.A.	Decl.	Duration	PSR	References
M53	20241007	13:12:55.00	+18:10:05.4	12900	M53A	Lian et al. (2023)
M3	20241003	13:42:12.00	+28:22:38.2	9900	M3B	Li et al. (2024)
	20240924	13:42:12.00	+28:22:38.2	11775	M3D	
	20240921	13:42:12.00	+28:22:38.2	10995	M3A	
M5	20220216	15:18:33.22	+02:04:51.7	7200	M5C, D	Zhang et al. (2023)
	20220211	15:18:33.22	+02:04:51.7	7200	M5A, B, E	
NGC 6517	20230929	18:01:51.52	−08:57:31.6	9000	NGC 6517D	Yin et al. (2024)
	20221231	18:01:51.00	−08:57:31.6	8400	NGC 6517A, B	
	20221228	18:01:51.00	−08:57:31.6	8400	NGC 6517C	
NGC 6539	20241009	18:04:50.00	−07:35:09.1	3000	NGC 6539A	Hobbs et al. (2004)
NGC 6760	20240930	19:11:02.1	+01:01:49.7	6600	NGC 6760A, B	Freire et al. (2005)
M71	20220530	19:53:44.00	+18:44:31.0	5285	M71A	Lian et al. (2025 in preparation)
M15	20231206	21:29:58.00	+12:10:01.2	13560	M15A to D	Wu et al. (2024)
	20220428	21:29:58.25	+12:10:01.23	7200	M15E to H	

The number of phase bins of search pulse is 128. For most of these 25 pulsars, the ephemerides that we obtained from either the PSRCAT (Manchester et al. 2005)[10] or publications are accurate enough for our FAST data. However, NGC 6760A exhibited a shift in its spin period. So, the routine PDMP from PSRCHIVE was used to search for the spin period. Since the effective bandwidth of 19-beam receiver is approximately 1.05–1.45 GHz, we removed the bands of 1.00–1.05 and 1.45–1.50 GHz using the PAZI routine of PSRCHIVE (Hotan et al. 2004).

According to the radio frequency interferences (RFIs) that were previously known in the FAST site (Zhang et al. 2020), namely the bands at 1085–1095, 1200–1215 and 1260–1285 MHz were also removed. Besides, we manually removed the obvious RFIs in time and frequency domains. In order to improve S/N in each frequency band, we scrunched the folded data into 256 sub-bands.

We subsequently conducted a standard polarization calibration procedure to account for the contributions of the telescope and observing system to the measured polarization. These effects are typically characterized by the Mueller matrix, M, as described in Lorimer & Kramer (2005) and represented in Equation (1).

$$M = M_{\rm amp} \times M_{\rm cc} \times M_{\rm PA}. \quad (1)$$

The Mueller matrix components were used to characterize specific instrumental and observational effects. The component $M_{\rm PA}$ accounts for the effect of the parallactic angle, with the feed of FAST fixed relative to the plane of polarization. $M_{\rm cc}$ represents the cross-coupling effect arising from the two orthogonal probes of the receiver. Given the minimal leakage between the two feeds of the 19-beam receiver, the single-axis model is accurate to within 0.04% (Ching et al. 2022). Finally, $M_{\rm amp}$ accounts for variations in gain and phase introduced by differences in the amplifier chains through which the signals pass. The polarization calibration was performed via the PAC routine in PSRCHIVE.

RM values were calculated for all observations using the RMFIT routine in PSRCHIVE software package. This method involves iteratively determining the differential position angle (ΔPA) of the linear polarization by splitting the data bandwidth into two half-bands. The relationship between ΔPA and RM is described by $\Delta{\rm PA} = \lambda^2 \times {\rm RM}$. We calculated the ionospheric contribution to the RM using IONFR, a code that estimates the ionospheric Faraday depth by incorporating publicly available global total electron content (TEC) maps and the most recent geomagnetic field model (Sotomayor-Beltran et al. 2013). Both the RM values before and after ionospheric correction are provided in Table 2.

3.2. Acquisition of Polarization Parameters

To optimize the S/N for each pulsar, we used PAM routine within PSRCHIVE software package to integrate the data in both time and frequency domains, generating high-quality mean pulse profiles. The polarization parameters were subsequently derived following steps detailed in Wang et al. (2023). From each averaged profile, we applied PDV routine in PSRCHIVE to obtain the measured Stokes parameters, I, Q, U and V. The on-pulse region is defined as the range of intensities exceeding three times the standard deviation of the baseline noise (3σ). Therefore, the linear ($L_{\rm on}$) and circular

[10] https://www.atnf.csiro.au/research/pulsar/psrcat/

Table 2
Polarization Measurements for GC Pulsars

PSR		Date	Integration Time s	P ms	DM pc · cm^{-3}	PB days	S/N	W_{10} °	W_{50} °	RM rad · m^{-2}	ionRM rad · m^{-2}	L/I %	V/I %	$\lvert V\rvert/I$ %
J1312+1810A	M53A	20241010	15660	33.16	25.03	255.86	341.0	40.1(9)	33.1(9)	−2(1)	−7(1)	56(1)	−21(1)	21(1)
J1342+2822A	M3A	20240921	10920	2.54	26.43	0.14	182.7	43.8(7)	25.2(7)	8(1)	3(1)	29(2)	1(3)	4(2)
J1342+2822B	M3B	20241003	9900	2.39	26.15	1.42	64.3	157.9(7)	22.0(7)	16(1)	9(1)	17(4)	2(6)	9(4)
J1342+2822D	M3D	20240924	11700	5.44	26.37	128.75	46.9	48.6(15)	20.3(15)	9(2)	3(2)	44(6)	−1(8)	9(5)
J1518+0204A	M5A	20220216	7200	5.55	30.05	*i*	909.5	50.2(16)	24.0(16)	−3(20)	−4(20)	19(1)	3(1)	5(1)
J1518+0204B	M5B	20220216	7200	2.95	29.47	6.86	124.0	193.3(8)	50.6(8)	−4(6)	−5(6)	4(5)	−6(7)	9(4)
J1518+0204C	M5C	20220211	7200	2.82	29.31	0.087	225.7	188.1(8)	155.6(8)	−1(2)	−2(2)	10(2)	0(3)	2(2)
J1518+0204D	M5D	20220211	7200	2.90	29.37	1.22	39.5	290.3(8)	73.0(8)	⋯	⋯	7(10)	11(14)	16(8)
J1518+0204E	M5E	20220216	7200	3.18	29.31	1.10	302.0	260.4(9)	99.3(9)	−2(8)	−3(8)	45(3)	3(3)	5(2)
J1801–0857A	NGC 6517A	20221231	8400	7.18	182.66	*i*	69.3	243.1(2)	73.7(2)	187(2)	183(2)	13(5)	2(8)	7(5)
J1801–0857B	NGC 6517B	20221231	8400	28.96	182.40	59.84	82.6	25.4(8)	12.8(8)	187(1)	183(1)	24(2)	−6(4)	6(3)
J1801–0857C	NGC 6517C	20221228	8400	3.74	182.36	*i*	45.2	327.0(1)	45.4(1)	212(2)	209(2)	5(8)	1(10)	10(6)
J1801–0857D	NGC 6517D	20230929	9000	4.23	174.54	*i*	37.8	299.9(1)	132.1(1)	189(2)	186(2)	27(11)	11(19)	18(12)
J1804-0735A	NGC 6539A	20241009	3000	23.10	186.32	2.62	1320.9	82.5(65)	21.6(65)	109(1)	106(1)	13(1)	−12(1)	13(1)
J1911+0102A	NGC 6760A	20240930	6600	3.62	202.68	0.14	302.7	105.7(10)	46.2(10)	129(4)	126(1)	31(2)	19(4)	20(2)
J1911+0102B	NGC 6760B	20240930	6600	5.38	196.69(2)	*i*	152.2	82.7(15)	24.1(15)	102(1)	99(1)	26(4)	1(5)	9(4)
J1953+1846A	M71A	20220530	5285	4.89	117.39	0.18	44.8	245.6(13)	43.9(13)	−480(14)	−481(14)	18(7)	−3(11)	10(6)
J2129+1210A	M15A	20220428	7200	110.66	67.23	*i*	1056.3	23.3(31)	8.8(31)	−72(1)	−74(1)	15(0)	−1(0)	4(0)
J2129+1210B	M15B	20220428	7200	56.13	67.73	*i*	96.5	56.0(16)	17.3(16)	−70(2)	−72(2)	24(4)	6(5)	10(3)
J2129+1210C	M15C	20220428	7200	30.53	67.10	0.34	4.1	⋯	⋯	⋯	⋯	⋯	⋯	
J2129+1210D	M15D	20230428	7200	4.80	67.28	*i*	80.2	199.2(14)	51.8(14)	−76(1)	−78(1)	13(8)	1(11)	11(7)
J2129+1210E	M15E	20231206	9664	4.65	66.59	*i*	80.0	113.8(13)	28.8(13)	−73(6)	−75(6)	20(5)	−3(6)	6(4)
J2129+1210F	M15F	20231206	9664	4.03	65.60	*i*	17.5	⋯	18.0(11)	⋯	⋯	4(11)	0(15)	15(10)
J2129+1210G	M15G	20231206	9664	37.66	66.40	*i*	11.5	⋯	⋯	⋯	⋯	⋯	⋯	⋯
J2129+1210H	M15H	20231206	9664	6.74	67.12	*i*	10.6	⋯	⋯	⋯	⋯	3(13)	−38(22)	37(15)

Note. DM values are extracted from references listed in Table 1. The RM and ionRM columns represent RM values before and after ionospheric corrected, respectively. The absence of RM and polarization ratios indicates that the S/N is not bright enough to determine its value.

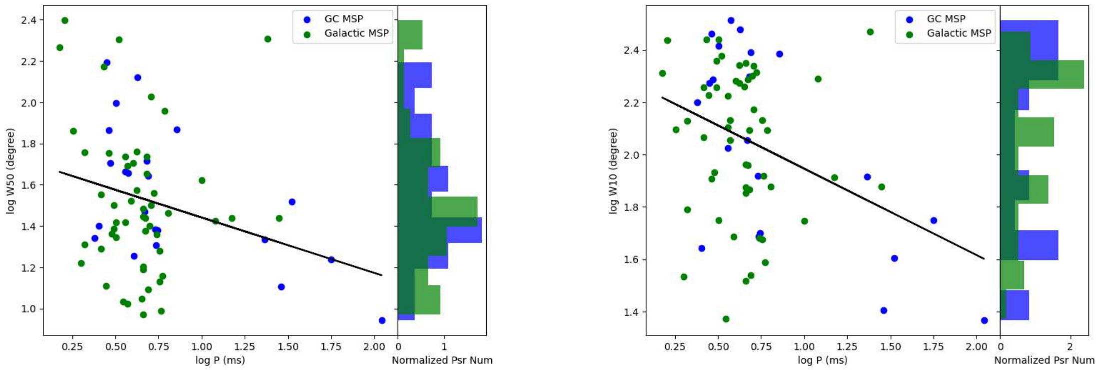

Figure 1. Panels on left and right are relationship between pulse width W_{50} or W_{10} with the period for pulsars. Blue points and bars represent GC MSPs, and green points and bars represent Galactic MSPs from Wang et al. (2023). Solid lines represent power-law fits to the data. For comparison, histograms on the right of each panel are accumulated normalized pulsar numbers.

($V_{\rm on}$) polarization for on-pulse bins is given by Weisberg correction:

$$L_{\rm on} = \begin{cases} \sqrt{L^2 - (\sigma_Q^2 + \sigma_U^2)} & \text{if } L^2 \geqslant \sigma_Q^2 + \sigma_U^2 \\ -\sqrt{(\sigma_Q^2 + \sigma_U^2) - L^2} & \text{otherwise.} \end{cases} \quad (2)$$

$$V_{\rm on} = \begin{cases} \sqrt{V^2 - \sigma_V^2} & \text{if } V^2 \geqslant \sigma_V^2 \\ -\sqrt{\sigma_V^2 - V^2} & \text{otherwise.} \end{cases} \quad (3)$$

The measured linear polarization, L is defined as $L^2 = Q^2 + U^2$. The uncertainties σ_Q, σ_U and σ_V correspond to the rms values of Q, U and V of the off-pulse region, respectively.

The polarization ratios, comprising the linear polarization ratio, circular polarization ratio, and absolute polarization ratio, were computed as $\sum L_{\rm on}/\sum I$, $\sum V_{\rm on}/\sum I$, and $\sum |V_{\rm on}|/\sum I$. The uncertainties of polarization ratios are calculated by following equations as detailed in Wang et al. (2023), where $N_{\rm on}$ represents the number of bins within the on-pulse region.

$$\sigma_{L/I} = \sqrt{N_{\rm on}[(\sigma_L/I)^2 + (L\sigma_I/I^2)^2]}, \quad (4)$$

$$\sigma_{V/I} = \sqrt{N_{\rm on}[(\sigma_V/I)^2 + (V\sigma_I/I^2)^2]}, \quad (5)$$

$$\sigma_{|V|/I} = \sqrt{N_{\rm on}[(\sigma_{|V|}/I)^2 + (|V|\sigma_I/I^2)^2]}, \quad (6)$$

We also applied PDV routine in PSRCHIVE software package to measure the pulse widths at 50% and 10% of the peak intensity of each profile. Following the convention in Kijak & Gil (1997), the uncertainties of pulse widths are given as $\sigma_W = t_b^2\sqrt{1 + (H/\sigma_I)^2}$, where t_b represents the time resolution of the phase bins in the profile and H is a scaling factor with values of $H = 0.5$ for W_{50} and $H = 0.1$ for W_{10}. These polarization parameters and uncertainties of polarization ratios and pulse widths are given in Table 2.

PAs were calculated using the relationship $\text{PA} = \frac{1}{2}\arctan(U/Q)$. The uncertainties in the PAs ($\sigma_{\rm PA}$) were determined through standard error propagation techniques. Only PAs with a confidence level greater than 3σ were retained.

4. Results and Discussion

4.1. Pulse Width

We compared the pulse width (W_{10} and W_{50}) distributions of the 25 GC pulsars in this work with those of a sample of MSPs in the GP from Wang et al. (2023). The comparison, shown in Figure 1, reveals that the two pulsar populations exhibit similar distributions for both W_{10} and W_{50}. Additionally, we examined the relationship between W_{10} and W_{50} with pulsar spin periods for GC pulsars and the same set of MSPs in the GP, as depicted in Figure 1. A power-law fit was performed for both GC and GP MSPs, yielding power-law indices of -0.268 (W_{10}) and -0.330 (W_{50}), respectively. For comparison, Karastergiou et al. (2024) reported a power-law index of -0.308 for the relationship between W_{10} and spin period, based on a sample that included both MSPs and slow pulsars observed with MeerKAT. Our results are consistent with the result of Karastergiou et al. (2024).

4.2. Profiles and Polarization

The polarization profiles for the 25 GC pulsars were presented in Figure 2. The corresponding polarization parameters were summarized in Table 2, including the fractions of linear polarization, circular polarization, the absolute value of circular polarization, W_{10} and W_{50}, and RM values. Among them, 10 were measured by Wang et al. (2023). Our results are

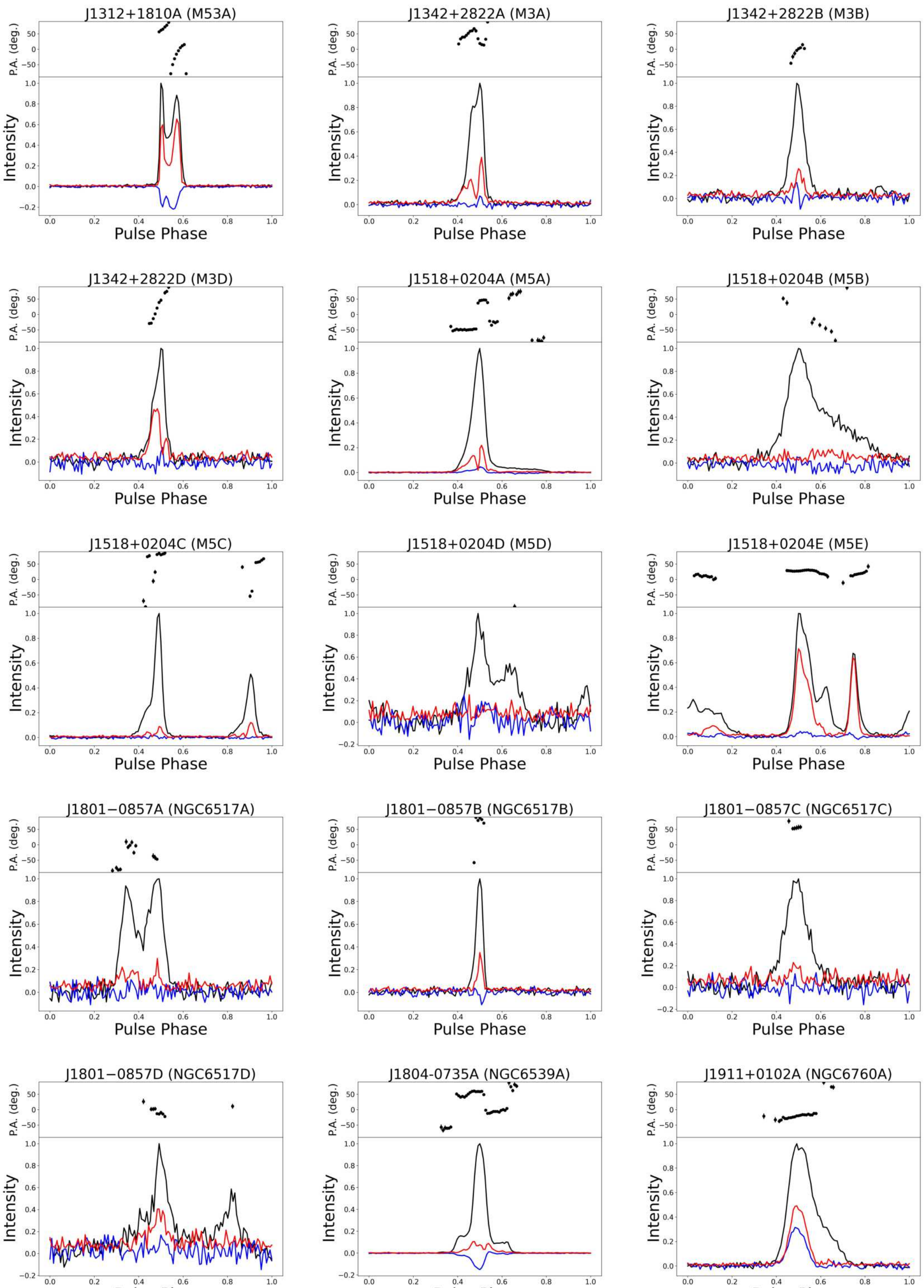

Figure 2. Polarization profiles of 25 GC pulsars. For each profile, the upper panel represents the PA. In the lower panel, the black line represents the total intensity, the red line represents the linear polarization, and the blue line represents the circular polarization. The pulsar names are in top of each panel.

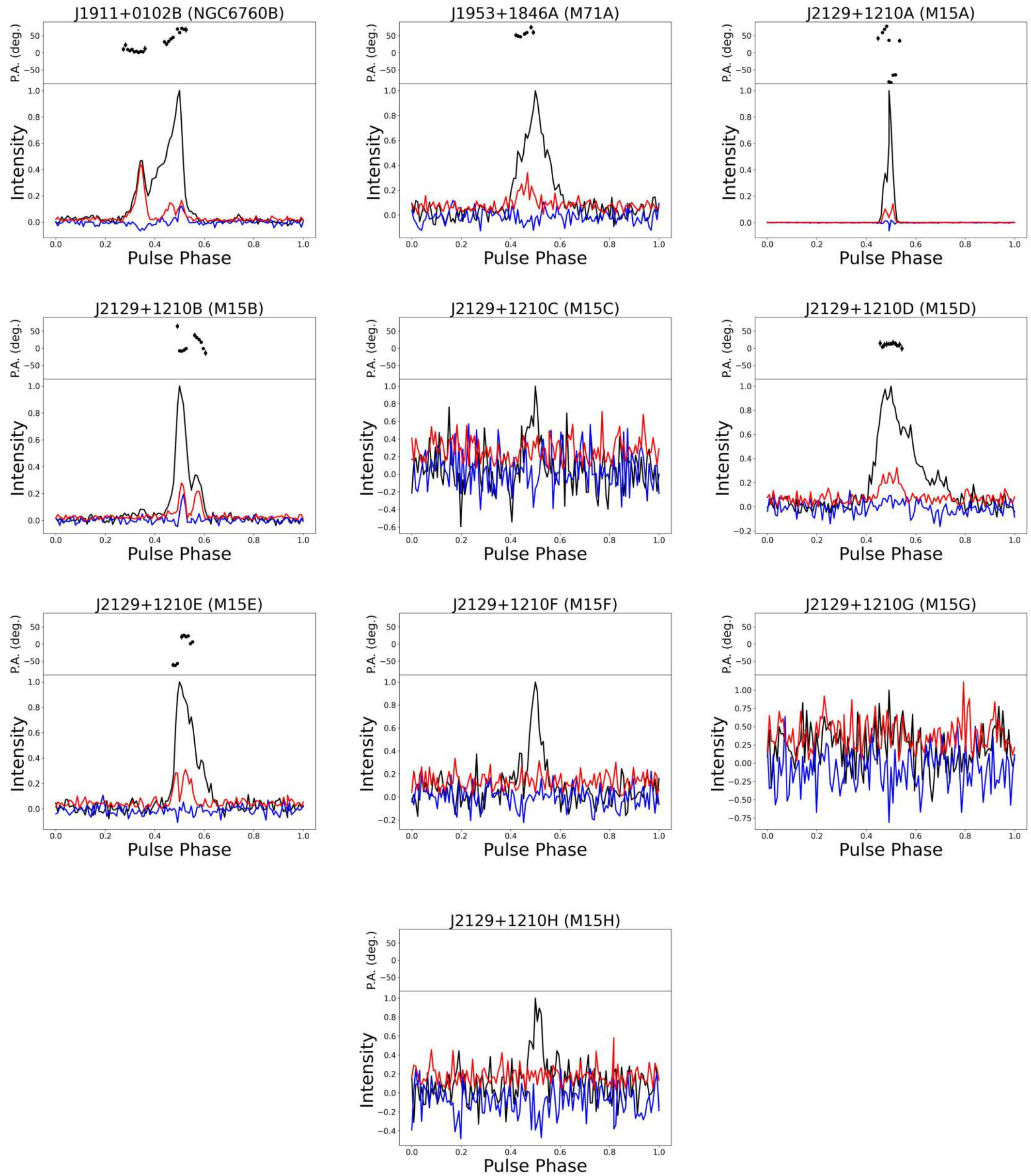

Figure 2. (Continued.)

consistent with their results. Notably, M15C is the only one residing in a double neutron star system. This pulsar exhibits a relatively long spin period (30.5 ms) and is characterized by a single, narrow pulse in its mean pulse profile. The polarization profile of M15C obtained from the 7200 s observation conducted on 2022 April 28, exhibits a lower S/N of 4, in contrast to the significantly higher S/N reported in the 2019 profile (from a 7320 s observation) by Wu et al. (2024). This disparity in S/N suggests that M15C may experience significant variability. This meets the prediction that the luminosity of M15C kept decreasing due to orbit variation (Ridolfi et al. 2017).

M5A, NGC 6539A and M15E exhibit orthogonal jumps at phase 0.5. M5A exhibits two linear polarization pulses within a single total intensity pulse. M5E exhibits a complex pulse profile, with linear polarization ratio in the third component reaching nearly 100%. Despite a 10.6 S/N of total intensity, M15H exhibits 37% absolute circular polarization ratio, being the highest among pulsars in this work. M53A and NGC 6760A also exhibit high circular polarization ratio, being

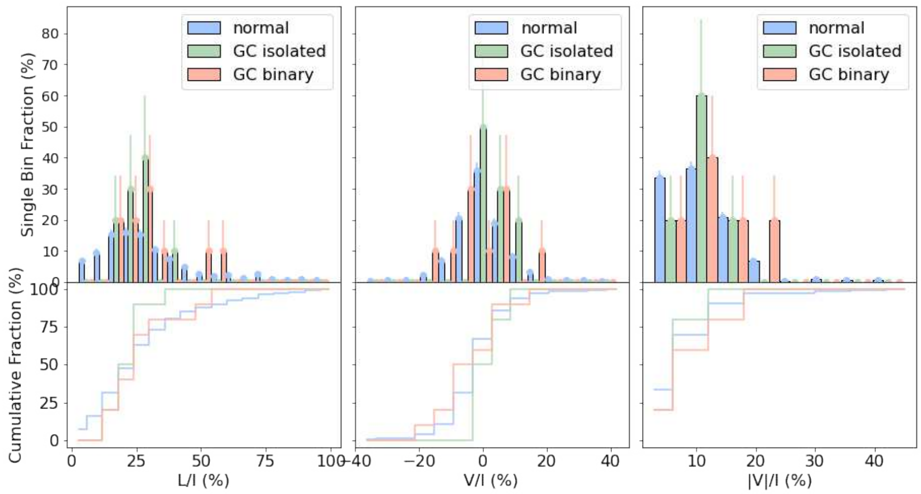

Figure 3. Histograms and cumulative distribution of polarization ratios for different pulsar categories. Normal pulsars are extracted from Wang et al. (2023), which are pulsars with periods greater than 50 ms and located in the GP.

−21% and 19%, respectively. Among the 25 GC pulsars, M5C, M5D, and M5E are the only three pulsars exhibiting inter-pulse emission, which is commonly attributed to radiation originating from the pulsar's opposite magnetic pole. Considering that M5C is an eclipsing black widow system, we measured the polarization profiles for each 5-minute integration across different orbital phases. However, we did not observe any significant variations in the polarization characteristics at these phases, in contrast to the behavior of PSR J1720-0533 reported by Wang et al. (2021) for the black widow J1720–0533.

4.3. Statistical Analysis

Pulsars M53A, M3A, M3B, M3D, and NGC 6760B exhibit significant S-shaped PA distributions, which can be well-modeled using the RVM. In contrast, more than 50% of slow pulsars display S-shaped PA variations that are consistent with RVM (Johnston et al. 2023). A similar proportion was reported by Karastergiou et al. (2024) for MSPs in the GP, based on observations conducted with MeerKAT. This discrepancy may underscore potential differences in the PA distributions of pulsars in GCs compared to those in the GP, while we emphasized that these differences may be caused by the small sample of GC pulsars, or more sensitive observations of a large sample of GC pulsars are needed.

The average ratios of linear, circular and absolute circular polarization of the 25 GC pulsars are 20%, −1%, 11%, respectively. Oswald et al. (2023) reported average polarization fractions of 28%, 5%, and 32% for linear, circular, and absolute circular polarization, respectively. This study was based on a sample of 271 pulsars, primarily slow pulsars located in the GP and observed with Parkes around 1400 MHz. In comparison, the average circular and absolute circular polarization fractions measured in this work are significantly lower than those reported for slow pulsars by Oswald et al. (2023). This discrepancy may reflect intrinsic differences in the polarization properties of pulsars in GCs compared to those in the GP. Again we emphasize that the small sample of GC pulsar may lead to these differences. Figure 3 depicts histogram and cumulative distribution of polarization ratios for slow pulsars, GC isolated pulsars and GC binary pulsars. Although the evolutionary processes of GC pulsars are influenced by the internal dynamics of GCs, differing from the evolutionary processes of MSPs in the Galactic disk, the results indicate that their polarization ratio distributions are consistent. The polarization ratio distribution of GC isolated pulsars appears slightly different from the others. We also suggest that our limited number of samples (25 pulsars) is the main reason. Future observations of more GC pulsars will be conducted to test this hypothesis.

RM values, as well as ionospheric-corrected RM values are measured and listed in Table 2. Pulsars in the same GC present similar RM values. For example, RM values of pulsars in M15 fall in the range of −70(2) to −76(1) rad m^{-3}. Pulsars in GCs such as M53 and M3 present low absolute RM values, ranging from 1 to 16 rad m^{-3}. M71A presents the largest absolute RM value, being as 481 rad m^{-3}. The distribution of GCs in the Galactic coordinate system is described in Figure 4, with RM values marked with different colors.

GCs farther from the GP, namely M53 and M3, show lower RM values, whereas those closer to the GP, such as M71 and NGC 6517, show relatively larger RM values. This result is consistent with the Galactic RM distribution reported by Hutschenreuter et al. (2022). Future work will involve measurements of more GC pulsars.

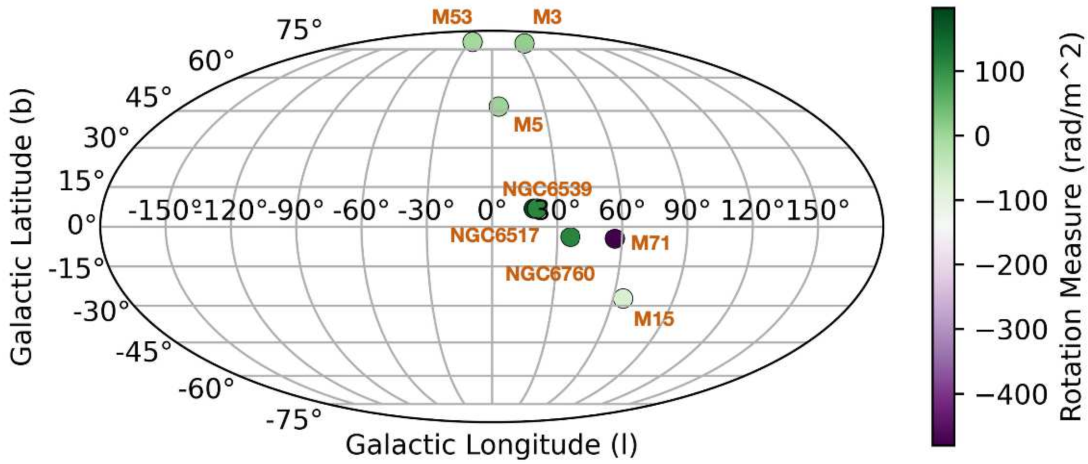

Figure 4. GC distribution with RM in Galactic coordinate system. The RM value for each GC is calculated as the average RM of pulsars within.

5. Conclusions

In this study, we measured polarization profiles of 25 pulsars in GCs with FAST, with 15 profiles being measured for the first time. The diversity of polarization profiles shows complex structure and emission pattern of pulsars. Power-law indices of W_{10} and W_{50} to the period for MSPs in GCs and GP are -0.268 and -0.330, respectively, being consistent with those of normal pulsars. Our analysis reveals that only 20% of the observed pulsars (M3A, M3B, M3D, M53A, and NGC 6760A) exhibit characteristic S-shaped PA curves, a significantly lower fraction compared to the population of normal pulsars (Johnston et al. 2023).

Linear, circular, and absolute circular polarization ratios are measured for each pulsar. M53A presents a 56% linear polarization ratio, being the highest among these 25 GC pulsars. M15H presents a 37% absolute circular polarization ratio, which is the highest among these 25 pulsars. The average ratios of circular and absolute circular polarization of these GC pulsars are -1% and 11%, respectively, lower than normal pulsars measured with Parkes (Oswald et al. 2023), which are 5% and 32%, respectively. Distribution of polarization ratios of the 25 pulsars is consistent with normal pulsars derived from Wang et al. (2023), indicating that the high stellar density environment in GCs may not affect the beam evolution of MSPs.

The ionospheric corrected RM values are measured for each GC pulsar. Pulsars in the same GC exhibit similar RM values. GCs closer to the GP tend to have larger RM, such as M71 and NGC 6517. This is consistent with previous studies given by Hutschenreuter et al. (2022).

We presented the polarization profiles of 25 pulsars, 26% of all 97 known GC pulsars in the FAST sky. Besides our study, on-going works are also on M2 (B. Li et al. 2025, in preparation), M13 (L. Wang et al. 2025, in preparation), M14 (K. Liu et al. 2025, in preparation), and NGC 6749 (P. C. C. Freire et al. 2025, in preparation). More GC pulsars still need public timing solutions (e.g., M92B[11]), or, with too high DM to be observed by FAST at the *L*-band (e.g., some pulsars in Glimpse C01[12]). Polarization studies on some of these pulsars will be reported in our next paper.

Acknowledgments

We sincerely appreciate the constructive comments provided by the reviewer. This work is supported by the National Key R&D Program of China, No. 2022YFC2205202 and the National Natural Science Foundation of China (NSFC) under grant Nos. 12173052, U2031119, 11773041 and 11703047. Zhichen Pan is supported by the Youth Innovation Promotion Association of the Chinese Academy of Sciences (CAS) (id. Y2022027); the CAS "Light of West China" Program, and the CAS President's International Fellowship Initiative (grant No. 2021FSM0004). This work made use of data from the Five-hundred-meter Aperture Spherical radio Telescope (FAST), a Chinese national mega-science facility operated by the National Astronomical Observatories, CAS. We appreciate the availability of publicly released FAST data and are grateful to Dejiang Yin, Yuxiao Wu, Baoda Li, and Yujie Lian for providing related data.

References

Abbate, F., Possenti, A., Ridolfi, A., et al. 2022, MNRAS, 518, 1642
Abbate, F., Possenti, A., Tiburzi, C., et al. 2020, NatAs, 4, 704
Ching, T. C., Li, D., Heiles, C., et al. 2022, Natur, 601, 49
Ferrière, K., & Terral, P. 2014, A&A, 561, A100
Freire, P. C. C., Hessels, J. W. T., Nice, D. J., et al. 2005, ApJ, 621, 959
Hobbs, G., Lyne, A. G., Kramer, M., Martin, C. E., & Jordan, C. 2004, MNRAS, 353, 1311
Hotan, A. W., van Straten, W., & Manchester, R. N. 2004, PASA, 21, 302

[11] https://fast.bao.ac.cn/cms/article/82
[12] https://www.trapum.org

Hutschenreuter, S., Anderson, C. S., Betti, S., et al. 2022, A&A, 657, A43
Jiang, P., Tang, N.-Y., Hou, L.-G., et al. 2020, RAA, 20, 064
Johnston, S., Kramer, M., Karastergiou, A., et al. 2023, MNRAS, 520, 4801
Karastergiou, A., & Johnston, S. 2007, MNRAS, 380, 1678
Karastergiou, A., Johnston, S., Posselt, B., et al. 2024, MNRAS, 532, 3558
Kijak, J., & Gil, J. 1997, MNRAS, 288, 631
Kou, F. F., Yan, W. M., Peng, B., et al. 2021, ApJ, 909, 170
Li, B., Zhang, L.-y., Yao, J., et al. 2024, ApJ, 972, 43
Lian, Y., Pan, Z., Zhang, H., et al. 2023, ApJL, 951, L37
Lorimer, D. R., & Kramer, M. 2005, Cambridge Observing Handbooks for Research Astronomers, 4 (Cambridge: Cambridge Univ. Press)
Lyne, A. G., Brinklow, A., Middleditch, J., et al. 1987, Natur, 328, 399
Lyne, A. G., & Manchester, R. N. 1988, MNRAS, 234, 477
Lyne, A. G., & Smith, F. G. 1968, Natur, 218, 124
Manchester, R. N. 1974, ApJ, 188, 637
Manchester, R. N., Hobbs, G. B., Teoh, A., & Hobbs, M. 2005, AJ, 129, 1993
Martsen, A. R., Ransom, S. M., DeCesar, M. E., et al. 2022, ApJ, 941, 22
Nan, R., LI, D., JIN, C., et al. 2011, IJMPD, 20, 989
Ng, C., Pandhi, A., Naidu, A., et al. 2020, MNRAS, 496, 2836
Oswald, L. S., Johnston, S., Karastergiou, A., et al. 2023, MNRAS, 520, 4961
Oswald, L. S., Weltevrede, P., Posselt, B., et al. 2025, arXiv:2504.09722
Pan, Z., Lu, J. G., Jiang, P., et al. 2023, Natur, 620, 961
Radhakrishnan, V., & Cooke, D. J. 1969, ApL, 3, 225
Rappaport, S., Putney, A., & Verbunt, F. 1989, ApJ, 345, 210
Ridolfi, A., Freire, P. C. C., Kramer, M., et al. 2017, in Proc. of IAU, 13, ed. P. Weltevrede et al. (Cambridge: Cambridge Univ. Press), 251
Sotomayor-Beltran, C., Sobey, C., Hessels, J. W. T., et al. 2013, A&A, 552, A58
van Straten, W., & Bailes, M. 2011, PASA, 28, 1
Wang, P. F., Han, J. L., Xu, J., et al. 2023, RAA, 23, 104002
Wang, S. Q., Wang, J. B., Wang, N., et al. 2021, ApJL, 922, L13
Wu, Y., Pan, Z., Qian, L., et al. 2024, ApJL, 974, L23
Xu, J., Jiang, J., Xu, H., et al. 2025, A&A, 695, A173
Yin, D., Zhang, L.-y., Qian, L., et al. 2024, ApJL, 969, L7
Zhang, H.-Y., Wu, M.-C., Yue, Y.-L., et al. 2020, RAA, 20, 075
Zhang, L., Freire, P. C. C., Ridolfi, A., et al. 2023, ApJS, 269, 56